Plenary Lectures (Alphabetical by Speaker)

Each Lecture is associated with a Session. Each Lecture may be accessed from this section or from the Associated Session. For each Lecture, links are provided for:

- **An abstract or extended abstract**
- **The speaker's slides**
- **A video of the full lecture**

Modeling of shells with three-dimensional finite elements
Manfred BISCHOFF *(University of Stuttgart)*
Associated Session: 3D Modeling of Thin-Walled Structures

Nanomechanical resonators and nanofluidic systems
Harold G. CRAIGHEAD *(Cornell University)*
Associated Session: Nano- and Micro-scale Structures

Analysis and design of materials and structures for attenuating vibration and acoustic response
Gregory M. HULBERT*, E. M. DEDE, C. YILMAZ, Z.-D. MA, Noboru KIKUCHI (University of Michigan)*
Associated Session: Dynamic Analysis of Spatial Structures

Large shell structures for power generation technologies
Wilfried B. KRÄTZIG *(Ruhr-University Bochum), Reinhard HARTE (University of Wuppertal), Ralf WÖRMANN (Krätzig & Partner)*
Associated Session: Spanning Between Theory and Practice

Answers to three not quite straightforward questions in structural stability
Andreas STEINBOECK, Gerhard HOEFINGER, Xin JIA, ***Herbert A. MANG*** *(Technical University of Vienna)*
Associated Session: Structural Stability

Computational morphogenesis: Its current state and possibility for the future
Hiroshi OHMORI *(Nagoya University)*
Associated Session: Computational Morphogenesis

Folding and deployment of stored-energy composite structures
Sergio PELLEGRINO *(California Institute of Technology)*
Associated Session: Deployable Structures and Biological Morphology

Rigid mechanics and its role in nonlinear structural analysis
Yeong Bin YANG *(National Taiwan University)*
Associated Session: Innovative Analysis Topics

For multiple-author papers:
Contact author designated by *
Presenting author designated by underscore

Proceedings of the 6th International Conference on
Computation of Shell and Spatial Structures
IASS-IACM 2008: "Spanning Nano to Mega"
28-31 May 2008, Cornell University, Ithaca, NY, USA
John F. ABEL and J. Robert COOKE (eds.)

Modeling of shells with three-dimensional finite elements

Manfred BISCHOFF

Institut für Baustatik und Baudynamik, Universität Stuttgart
Pfaffenwaldring 7, D-70550 Stuttgart, Germany
bischoff@ibb.uni-stuttgart.de

Abstract

Some aspects of three-dimensional analysis of shells are discussed, comparing 3d-shell formulations, surface oriented shell formulations and three-dimensional solid elements ("bricks"). Comparison is made with respect to theoretical formulation, finite element technology and consistency. Advantages and drawbacks of the different concepts are discussed, distinguishing the case of thin shells, where locking effects play a prominent role, and the analysis of three-dimensional structures ("very thick" shells). In this context a fundamental dilemma appears, namely the impossibility to design an element which is completely free of locking and passes the patch test at the same time.

1. Introduction

Finite element analysis of shells is a standard procedure in many engineering applications. Throughout the past fifteen years significant progress has been made in the field of three-dimensional shell theories and related finite elements (also called "solid shell" elements). The main benefits are approximate consideration of three-dimensional stress states, ease of implementation of three-dimensional constitutive laws and simplicity (no rotational degrees of freedom involved).

Sometimes application of shell finite elements is totally abandoned in favor of a discretization with three-dimensional solid finite elements. Standard 3d-solid finite elements, however, are often not suited to predict the behavior of shells properly. Locking effects may lead to significant errors for thin shells. Even well-established "locking-free" solid elements may fail in thin shell analysis. The problem can be avoided by transferring concepts of finite element technology from (3d) shell elements to solid elements.

A particularly interesting phenomenon in this context is *trapezoidal locking* (also called *curvature thickness locking* in the context of 3d-shell elements) and its relationship to passing the constant stress patch test. There are strong indications that obtaining a locking-free formulation and passing the patch test are mutually exclusive (a result already anticipated by Richard MacNeal in a discussion about distortion sensitivity of finite elements).

2. Three different archetypes of three-dimensional elements for shell analysis

Without going into technical details of mathematical formulations, three different philosophies for designing finite elements which are feasible for both thick and thin shell analysis, using unmodified three-dimensional constitutive laws are described in this section (see Figure 1 for an illustration).

3d-shell finite elements have become popular (particularly in Germany) at the beginning of the 90s, the works of Simo et al. [4] and Büchter et al. [4] being two of the decisive pioneering contributions. They rely on the classical concept of a mid-surface, equipped with displacement degrees of freedom, rotations (or difference displacements) as well as some higher order parameters, for instance describing the thickness change of the shell. A typical representative of this class is a so-called *7-parameter formulation*, utilizing three displacements of the mid-surface, three components of a difference vector (naturally including a constant thickness stretch) plus one additional strain (or displacement) parameter to realize a linear distribution of transverse normal strains. The latter is necessary to avoid *Poisson thickness locking* or, in other terms, to make the formulation asymptotically correct for bending.

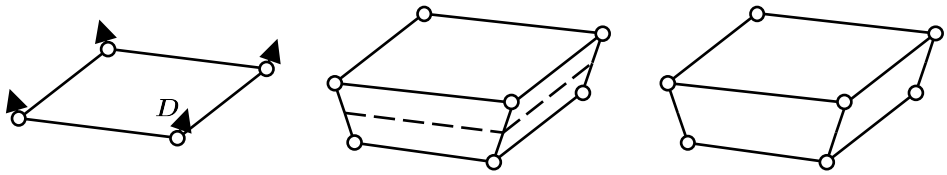

Figure 1: 3d-shell, surface oriented shell and "shell-like" 3d-solid

Unless the three-dimensional constitutive equations are somehow manipulated, all strain components need to be linear through the thickness in order to correctly model bending. In this spirit, quadratic terms are not needed for an asymptotically correct shell model and they are usually dropped from the formulation. Contribution of these higher order terms to the strain energy is negligible in most cases. This assumption is commonplace for practically all classical and three-dimensional shell models.

The mechanical ingredients of *surface oriented* shell formulations are identical to those of 3d-shells. The decisive difference is the usage of a three-dimensional parameterization of geometry and displacements with *absolute* values for position vectors and displacements rather than working with a director field $\boldsymbol{D}$ and difference displacements $\boldsymbol{w}$, see Figure 2. Surface oriented shell finite elements may be seen as hybrids of three-dimensional finite elements and shell elements. From the former they inherit their "outer appearance", i.e. geometry and nodal degrees of freedom. And from the latter the "inner life" is deduced, particularly the use of stress *resultants* (membrane forces, bending moments etc.), rather than stresses and the aforementioned reduction strains to linear functions in thickness direction.

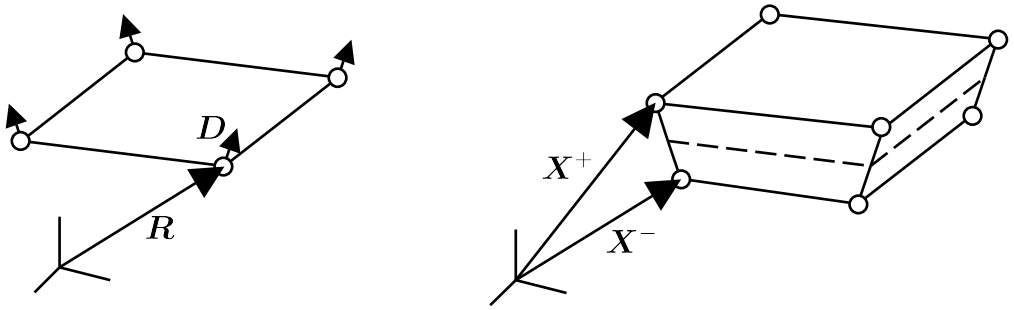

Figure 2: "classical" 3d-shell versus surface oriented 3d-shell

The concept of a surface-oriented shell model described in the previous section implies the question why not simply using 3d-elements for shell analysis. The nodal degrees of freedom are exactly the same and the 7th parameter is naturally included in many 3d-solid finite elements by certain means of element technology which are needed to avoid volumetric locking (EAS, Simo and Rifai [4]). The decisive differences of three-dimensional solid elements compared to three-dimensional (or surface oriented) shell elements are

1. that there are no distinct "in-plane" and "thickness" directions and
2. three-dimensional strains and stresses, rather than "resultants" are used, i.e. there are no separate expressions for membrane strains, curvatures, bending moments or transverse shear forces.

As a consequence, in a three-dimensional finite element the quadratic terms of the through-the-thickness strain distribution are not skipped – they *cannot* be skipped, because they do not appear separately. This is not a disadvantage because it does not affect computational cost. It may be even advantageous to have these terms included, as we will see later.

There is, however, a drawback in comparison to shell elements: From the point of view of element technology it is desirable to distinguish in-plane and out-of-plane strain and stress components, (e.g. when special formulations ought to be applied to avoid *transverse* shear locking or trapezoidal locking) as well as constant and linear ones (e.g. membrane and bending strains when membrane locking ought to be avoided). In fact, the crucial problem is trapezoidal locking (related to transverse normal strains) as will be demonstrated in the next section.

3. Trapezoidal locking and the patch test

We compare, in a numerical experiment, performance of state of the art solid elements and shell elements. A cylindrical shell with clamped boundaries is subject to uniform external pressure. A linear pre-buckling analysis is performed, based on solving the corresponding eigen value problem. Two different setups are considered: a relatively thick shell, with a radius-to-thickness ratio of 100 and a thin shell with slenderness 500. The commercial finite element package ANSYS is used as solver. The solid elements implemented in ANSYS use the enhanced assumed strain method, representing widely used, and state of the art brick elements. Comparison is made to a solution using conventional Kirchhoff-Love type shell elements which are free from locking for the problem at hand (similar results are obtained with well-formulated 3d-shell elements).

	mesh	shell elements	solid elements
thick shell	coarse	$\lambda_{crit.} = 1.02$	$\lambda_{crit.} = 1.7$
	fine	$\lambda_{crit.} = 1.0$ (reference)	$\lambda_{crit.} = 1.02$
thin shell	coarse	$\lambda_{crit.} = 1.02$	$\lambda_{crit.} = 13.0$
	fine	$\lambda_{crit.} = 1.0$ (reference)	$\lambda_{crit.} = 1.7$

Table 1: Critical load factors for thick and thin shell, fine and coarse meshes

The numerical results, normalized with respect to the fine mesh shell solution are summarized in Table 1. The coarse meshes use 4608 degrees of freedom (in both shell and solid discretizations) and the fine mesh involves 18816 d.o.f. It can be seen that the coarse mesh solution using shell elements is already satisfactory, while the coarse mesh solution with solid elements is unacceptable in both cases (thick and thin cylinder). Moreover, the absolute errors are much larger for the thin cylinder in the solid element solutions – a typical symptom of locking. Note, that even for the fine mesh the critical load is overestimated by 70 %. Figure 3 shows that the solid elements do not only overestimate the buckling load but also predict a wrong buckling pattern.

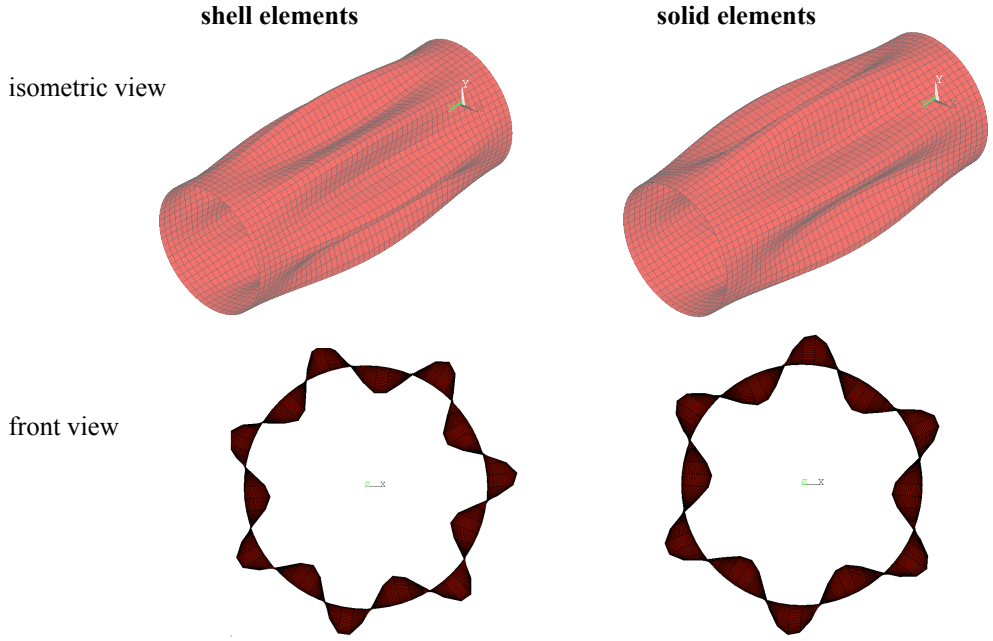

Figure 3: Comparison of buckling modes for shell elements and solid elements

Analyzing the problem setup and the involved element formulations one can identify trapezoidal locking as the reason for the observed behavior. Within a three-dimensional or surface oriented shell formulation it can be avoided following the idea of Betsch et al. [4] (see also Bischoff and Ramm [4]), modifying the constant part of

the transverse normal strains ε_{33} by an ANS formulation. As there is no "transverse" direction in a 3d-solid, transferring this concept is not straightforward. If one strives to keep element technology "isotropic", all normal strain components ought to be modified accordingly. This works fine for the numerical experiment documented in this section, but the resulting elements fail to pass the constant strain patch test. Strictly speaking, this means that these elements are not consistent and thus not convergent – a fact that is mostly considered unacceptable. The same holds for typical methods to avoid transverse shear locking.

We conclude that there is no way around an "anisotropic" element technology for 3d-solids, if these are expected to work as well as (3d) shell elements in the case of thin shells. This means that a certain thickness direction has to be nominated and the finite element formulation is adapted accordingly. If transverse shear strains and transverse normal strains are treated such that transverse shear locking and trapezoidal locking are avoided, 3d-solid elements may be used as efficiently as 3d-shell elements for thin shell analysis. These elements pass the patch test as long as the elements are distorted "in-plane", but still not in general three-dimensional situations. To be more precise: Constant strain states cannot be exactly represented if the thickness direction is not orthogonal to the other two directions.

The special treatment of transverse normal strains to avoid trapezoidal locking is one of the reasons for this problem. This observation is closely related to a discussion about distortion sensitivity of finite elements and passing the patch test, put forward by Richard MacNeal [4]. Removing these "tricks" from the element formulation leads to an element that passes the patch test (of course, trapezoidal locking re-enters the formulation).

For a surface oriented shell element the patch test is still not passed in this case. The reason is omitting the quadratic terms of the strain distribution trough the thickness. These are needed for exact representation of constant stress states for arbitrary meshes, because the metric is changing through the thickness.

One way out of this dilemma may be to accept the fact that the elements do not pass the patch test and favor formulations which are locking-free. Consistency, and thus convergence, may be achieved in a weaker sense by ensuring that those element distortions which are responsible for not passing the patch test vanish with mesh refinement. As these are related to deviation of the shell director from the shell normal, this seems to be a feasible approach.

3. Summary

Formulation of locking free 3d-solid elements for shells still has potential for improvement. Avoiding all locking effects and passing the patch test at the same time seem to be mutually exclusive. Standard "locking-free" 3d-solid elements usually suffer from trapezoidal locking and are therefore not suited for general shell analysis. The situation can be improved with an anisotropic element technology. Surface oriented shell elements use stress resultants and thus methods of element technology may be applied more purposeful.

References

[1] P. Betsch. F. Gruttmann, E. Stein. A 4-node finite shell element for the implementation of general hyperelastic 3d-elasticity at finite strains. *Computer Methods in Applied Mechanics and Engineering*, **130**:75-79, 1995.

[2] M. Bischoff, E. Ramm. Shear deformable shell elements for large strains and rotations. *International Journal for Numerical Methods in Engineering*, **40**:4427-4449, 1997.

[3] N. Büchter, E. Ramm, D. Roehl. Three-dimensional extension of non-linear shell formulation based on the enhanced assumed strain concept. *International Journal for Numerical Methods in Engineering* **37**:2551-2568, 1994.

[4] R. MacNeal. *Finite Elements: Their Design and Performance*. Marcel Dekker, 1994.

[5] J.C. Simo, S. Rifai. A class of mixed assumed strain methods and the method of incompatible modes. *International Journal for Numerical Methods in Engineering*, **29**:1595-1638, 1990.

[6] J.C. Simo, S. Rifai, D. Fox. On a stress resultant geometrically exact shell model. Part IV: variable thickness shells with through-the-thickness stretching. *Computer Methods in Applied Mechanics and Engineering*, **81**:91-126, 1989.

Proceedings of the 6th International Conference on
Computation of Shell and Spatial Structures
IASS-IACM 2008: “Spanning Nano to Mega”
28-31 May 2008, Cornell University, Ithaca, NY, USA
John F. ABEL and J. Robert COOKE (eds.)

Nanomechanical resonators and nanofluidic systems

Harold G. CRAIGHEAD*

*Charles W. Lake, Jr. Professor of Engineering
Professor of Applied and Engineering Physics
Director, Nanobiotechnology Center
Cornell University
hgc1@cornell.edu

Abstract

We have explored the properties and applications of small-scale mechanical resonators and fluidic devices. Studied systems include lithographically defined structures in a range of geometries, including nanotubes, nanostrings, and membranes as thin as a single sheet of carbon. While we have employed a variety of mechanical actuation techniques, we have found that optical methods for both actuation and motion transduction have proven remarkably robust and applicable to even the smallest resonant structures. With larger dimensioned structures we have examined some of the practical issues of detection of particulate binding and detachment using resonant motion. Nanofluidic systems have been used for single molecule analysis and controlling the confirmation and position of individual DNA molecules. The fabrication, properties and applications of these systems as sensors and analytical devices will be discussed.

Proceedings of the 6th International Conference on
Computation of Shell and Spatial Structures
IASS-IACM 2008: "Spanning Nano to Mega"
28-31 May 2008, Cornell University, Ithaca, NY, USA
John F. ABEL and J. Robert COOKE (eds.)

Analysis and design of materials and structures for attenuating vibration and acoustic response

Gregory M. HULBERT*, Ercan DEDE, Cetin YILMAZ, Zheng-Dong MA, Noboru KIKUCHI

*University of Michigan
Ann Arbor, Michigan 48109-2125
Hulbert@umich.edu

Abstract

The ability to design to design and manufacture materials with complex structure and novel material response offers the opportunity to consider the control of the dynamic response of structures. This problem is well suited for a multi-scale approach in which the material characteristics and material layout are considered as part of the structural analysis and design problem.

Three approaches towards the design of band-gap materials and structures are presented and representative materials and structures are shown. In addition to material design employing Bragg scattering, the use of compliant mechanisms in sandwich structures is demonstrated. Lastly, inertial amplification is shown to provide a third method of inducing band-gap phenomena into materials and structures using embedded amplification mechanisms.

1. Introduction

The importance of designing structures with desired dynamic response characteristics is increasing, particularly in the ground vehicle industry. This is driven by customer demands for quiet vehicles and for well-tuned ride characteristics. In addition, safety requirements also are impacted by the dynamic response of materials, especially for military vehicles. Competing with these requirements is the continuing need to reduce the weight of vehicles to improve fuel economy. To this end, significant research has been directed towards the design of new composite materials.

Of particular focus in the present work is to construct systematically materials that enable structures to have designed vibration or acoustic response (spectral gaps) or to have significantly reduced response in desired frequency bands. Using a multi-scale approach, the desired structural response can be obtained by careful design of the material response.

Spectral gaps in the band structure of periodic media have been an ongoing research endeavor since the 1950s. In the last decade, there has been growing interest in computing and designing the phononic band structure of 2D and 3D periodic systems comprising various materials. Of particular focus has been obtaining complete phononic band gaps, which forbid the propagation of elastic or acoustic waves regardless of mode or wave vector. Practical applications of these systems include mechanical filters, sound and vibration isolators, and acoustic waveguides.

The two different widely published means of generating phononic band gaps in periodic media are Bragg scattering and local resonances. In Bragg scattering, a gap appears due to destructive interference of the wave reflections from the periodic inclusions within the media. Band gaps can also be generated via local resonators, which impede wave propagation around their resonance frequencies. A third approach towards phononic band gap generation is possible in which the effective inertia of the wave propagation medium is amplified via embedded amplification mechanisms. We classify this alternate approach as inertial amplification.

These three approaches towards the design of band-gap materials and structures are presented and representative materials and structures are shown. In addition to material design employing Bragg scattering, the use of compliant mechanisms in sandwich structures is demonstrated as a novel application of local resonances. Lastly, inertial amplification is shown to provide a third method of inducing band-gap phenomena into materials and structures using embedded amplification mechanisms.

2. Bragg scattering

Wave propagation in heterogeneous media is dispersive, i.e., the media causes an incident wave to decompose into multiple waves with different frequencies. A medium with periodic heterogeneity has distinct frequency ranges in which waves are either effectively attenuated or allowed to propagate. These frequency ranges are referred to as *band-gaps* (or stop bands) and *bands* (or pass bands), respectively, and are attributed to mechanisms of wave interference within the scattered elastic field, known as Bragg scattering. From a practical perspective, it has been shown that under certain conditions bounded structures formed from periodic materials can exhibit similar frequency-banded wave motion characteristics. By controlling the layout of constituent material phases and the ratio of their properties within a unit cell, a periodic composite can be designed to have a desired frequency band structure (the size and location of stop bands and pass bands). Figure 1 depicts various designs of a bi-material unit cell that exhibit different frequency band-gap responses. In Hussein *et al*. [1], an optimization problem was constructed to identify unit cell topologies that could maximize the bandwidth of the stop-band behavior across a broad frequency response domain.

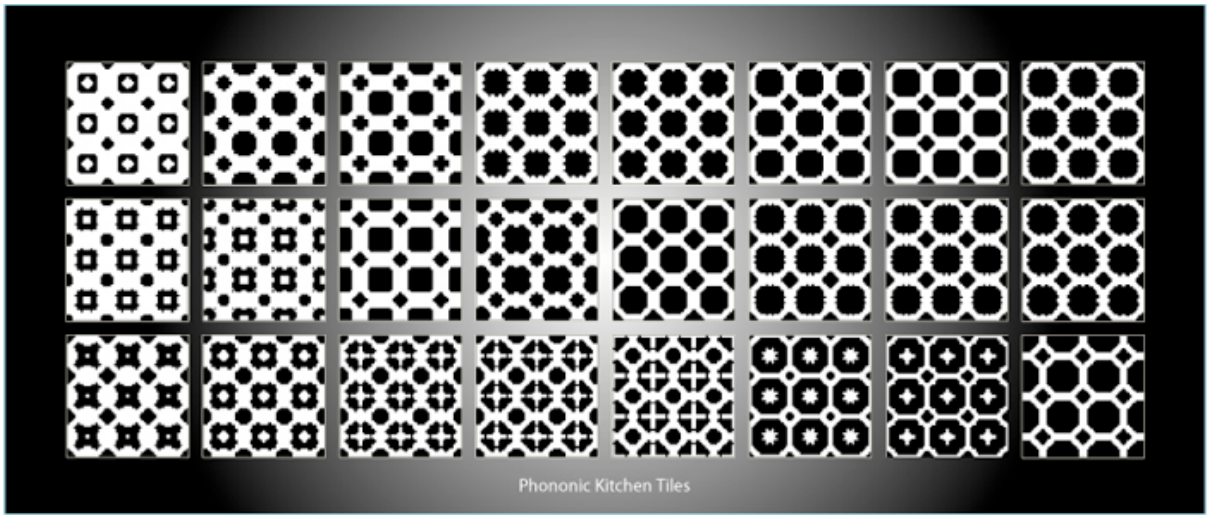

Figure 1: Examples of bi-material layouts to optimize phononic band-gaps using Bragg scattering (courtesy of Prof. Mahmoud I. Hussein)

3. Integral compliant mechanisms

The design of structures to mitigate structural vibration and acoustic response in mid-frequency spectrums (1-10 kHz) often has relied upon periodic lattices and structures, in particular, sandwich structures. The high stiffness-to-weight ratio and mid-frequency isolation attributes of sandwich structures both are attractive for the design of practical engineering structures. We have explored the novel use of compliant mechanisms as the core topology to attenuate mid-frequency structural response of sandwich structures; see, e.g., Dede and Hulbert [2]. While compliant mechanisms have been an active research field for the past 20 years, their application as a building block for vibration attenuation of sandwich structures presents a new application field. Figure 2 depicts an optimized compliant cell unit topology and a sandwich structure constructed from an assembly of the unit cells. The ability to optimize the compliant mechanism topology is described in Dede and Hulbert [2].

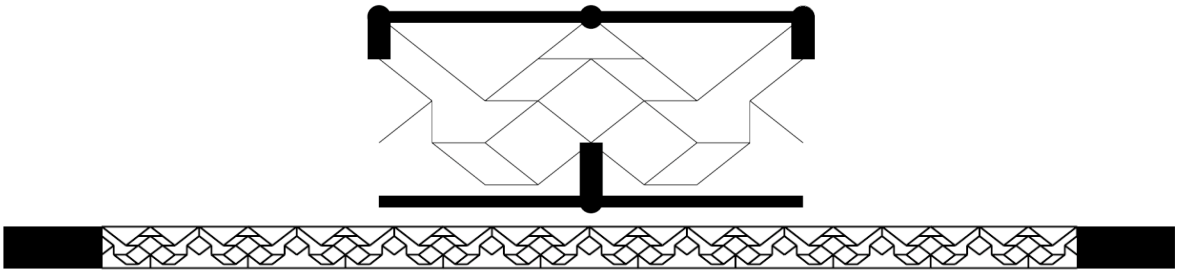

Figure 2: A reduced unit cell compliant mechanism topology (top); compliant sandwich structure comprising ten parallel unit cells (bottom).

4. Inertial amplification

A significant and practical challenge is to design systems that possess wide, low-frequency band-gaps. The lowest frequency gap due to Bragg scattering is of the order of the wave speed (longitudinal or transverse) of the medium divided by the lattice constant. Thus, a low-frequency Bragg gap requires low wave speeds (i.e., heavy inclusions in a soft medium) or a large lattice constant. On the other hand, by choosing low resonator frequencies, one can place local resonator induced band-gaps at much lower frequencies than that can be obtained by Bragg scattering. Low-frequency local resonances can be realized by embedding rubber-coated dense metal spheres or cylinders in an epoxy matrix. However, to obtain wide band-gaps at low frequencies, large volume filling fractions are required. Since the average density of the coated inclusions, e.g., rubber and dense metal, is more than an epoxy matrix, large volume fractions imply even larger mass fractions. Consequently, to obtain wide band-gaps at low frequencies, heavy resonators are needed that form a large fraction of the overall mass of the medium. Alternatively, by amplifying the effective inertia of the wave propagation medium using embedded amplification mechanisms, it is possible to circumvent the disadvantages described.

One of the first designs that made use of amplified effective inertia employs a single stage vibration isolator consisting of a levered mass in parallel with a spring. Such systems are used to isolate massive objects from vibrations. The lever in the system generates large inertial forces by amplifying the motion of a small mass, which in turn effectively increases the inertia of the overall system by lowering its resonance frequency. Furthermore, the isolator also introduces an anti-resonance frequency when the inertial force generated by the levered mass cancels the spring force. In Yilmaz *et al*. [3], this inertial amplification concept is utilized to generate band-gaps in infinite periodic systems. Their simple yet effective geometry allows them to be easily embedded into two or three-dimensional lattices, as illustrated in Figure 3. It is shown that the widest low-frequency band-gaps are obtained when most of the mass within the lattice is concentrated on very stiff amplifiers that can generate large amplifications. However, with smaller mass fractions on amplifiers, wide low-frequency band-gaps can still be obtained, provided that amplifiers are moderately stiff and can generate reasonably large amplifications. This is in contrast to obtaining wide low-frequency gaps via local resonators, which require heavy resonators that form a large fraction of the overall mass of their unit-cell. Moreover, unlike Bragg scattering, wave speeds and the lattice constant do not limit the lower frequency limit of a band-gap. Hence, this alternative method of generating band-gaps is particularly attractive for low-frequency applications.

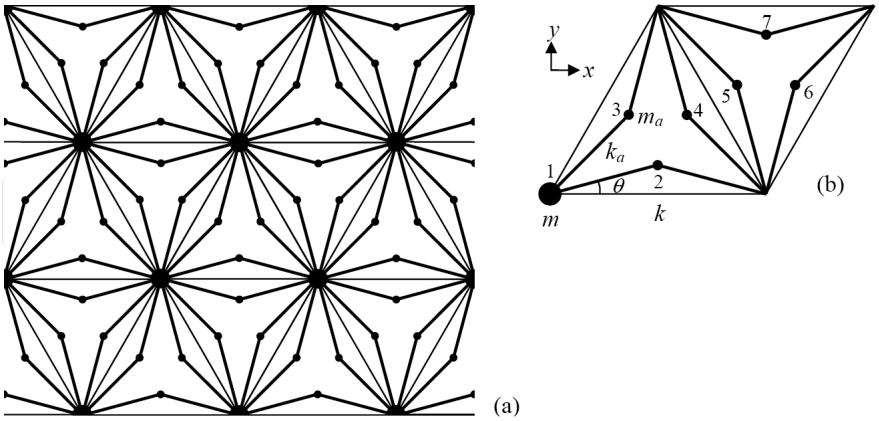

Figure 3: The infinite periodic lattice with inertial amplification (a); its irreducible unit cell (b).

References

[1] Dede EM, Hulbert GM. Analysis, design and optimization of structures with integral compliant mechanisms for mid-frequency response. *International Journal for Numerical Methods in Engineering* 2008; **73**: 470-492.

[2] Hussein MI, Hamza K, Hulbert M, Saitou K. Optimal synthesis of 2D phononic crystals for broadband frequency isolation. *Waves in Random and Complex Media* 2007; **17**: 491-510.

[3] Yilmaz C, Hulbert GM, Kikuchi N. Phononic band gaps induced by inertial amplification in periodic media. *Physical Review B* 2007; **76**: 054309.

Proceedings of the 6th International Conference on
Computation of Shell and Spatial Structures
IASS-IACM 2008: "Spanning Nano to Mega"
28-31 May 2008, Cornell University, Ithaca, NY, USA
John F. ABEL and J. Robert COOKE (eds.)

Large shell structures for power generation technologies

Wilfried B. KRÄTZIG*, Reinhard HARTE[1], Ralf WÖRMANN[2]

* Ruhr-University Bochum, Universitätsstrasse 150, D-44780 Bochum, wilfried.kraetzig@rub.de
[1] University of Wuppertal, Pauluskirchstrasse 7, D-42285 Wuppertal, harte@uni-wuppertal.de
[2] Krätzig & Partner Engg. Comp., Buscheyplatz 9-13, D-44801 Bochum, woermann@kraetzigundpartner.de

Abstract

In power generation industries large RC shell-like structures are well in use, as safety containments for LNG tanks, shafts for wind generators, smoke stacks, nuclear power plant containments, natural draft cooling towers, and in future solar upwind chimneys. Especially these last two types of shells form the largest shell structures in technology. Because of their size they are extremely exposed to storms and to seismic actions. Since attacked by environmental effects, the damage evolutions determine to a large extend their service-lives. Many structural phenomena, like forced vibrations, static and dynamic instabilities, or damage-induced failure, influence their safety and reliability. The present lecture will address some of these typical mechanical effects of large "wet" as well as "dry" natural draft cooling towers and for chimneys of solar upwind power plants.

1. "Wet" natural draft cooling towers

Due to the rising demand for cheap, economic as well as sustainable electricity, natural draft cooling towers (NDCT) at the "cold ends" of thermal power generation processes, have grown to enormous sizes and heights. Simultaneously, their shells developed to the largest reinforced concrete (RC) shell structures in technology. Compared to shell roofs or tanks, NDCTs are exposed on both faces to aggressive fuel combustion media. Additionally, aggressiveness in the towers' interiors is increased in Germany by release of cleaned flue gases therein, saving former customary smoke stacks (Krätzig *et al.* [3]).

So in addition to classical design conditions for load combinations of deadweight G, wind W, internal suction S, service temperature T, hygro-thermal attack H, and probably seismic actions E, durability is the key issue in the design of NDCTs. Possible structural shell repairs are limited to rather short shut-downs of the plant. Even in case of surfaces up to 60.000 m² each side for modern towers, sufficiently long shut-downs for careful surface repairs are illusionary.

The paper will report in detail on typical structural design efforts for cooling tower shells of extreme size, namely the shape optimization of the meridian, the construction of the flue gas inlet, the application of special acid-resistant high-performance concrete, and on design concepts to increase the shells' durability.

Here we describe the constituents of such huge wet NDCTs by example of the world-largest tower of 200 m of height at the RWE Power Station Niederaussem, some 20 km west of Cologne. Figure 1 shows the entire plant during construction in the year 2000. The new lignite power block BoA (left) has a net capacity of 965 MW, achieved by an efficiency of over 43%, the highest electrical net degree of efficiency of lignite fueled power plants worldwide. The 200 m cooling tower contributes considerably to this world record (Busch *et al.* [2]).

As confirmed in Figure 2, the total height of the cooling tower shell is 200 m. Its water basin diameter measures 152.54 m, that one of the lower shell rim 136.00 m, and the top opening is 88.41 m wide. Both the outer and inner shell faces measure about 60.000 m², equivalent to 10 soccer fields each. The tower shell is composed of two hyperbolic shells of revolution, meeting at the throat. It exhibits largely a wall thickness between 0.22 and 0.24 m, increasing towards the lower shell rim. The top edge of the shell is stiffened by an upper edge member with U-shaped cross-section, extending into the interior. The overhang measures 1.51 m with a shank-height of 1.20 m. To reduce crack-sensibility of the upper shell due to wind vibration, this edge member is pre-stressed by

Figure 1: Power Station Niederaussem (Photo RWE)

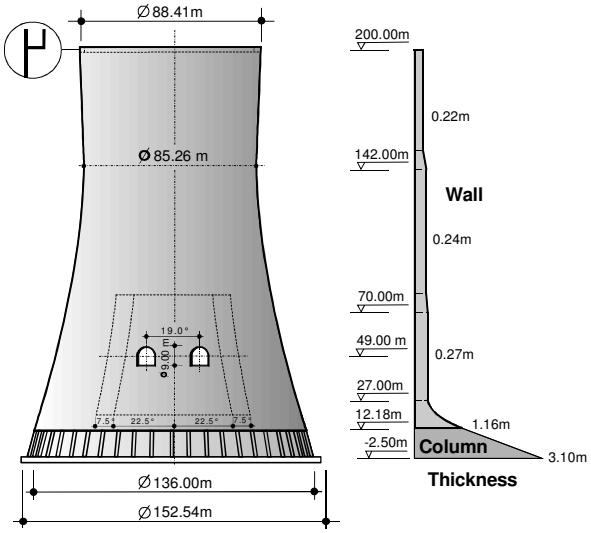

Figure 2: Dimensions of NDCT Niederaussem

4 SUSPA tendons with 8 mono-wires of 150 mm² cross-section each of steel quality St 1570/1770 N/mm². The lower edge member is formed by an increase of the shell thickness up to 1.16 m. The complete shell is made from acid-resistant high-performance concrete of compression strength of 85 N/mm², so-called ARHPC 35/85, to save a protective coating of the inner surface.

The cooling tower shell is supported by 48 meridional columns of 14.68 m of height, cast of RC 45/55 due to Eurocode EC 2. Their thickness ranges from 1.16 m on top to 3.10 m above foundation, their width is 1.40 m. All columns rest on a RC ring foundation of 6.60 m of width and 1.80 m of height. Softer soil than the standard consolidated gravel was exchanged. Along the water inlets and the water outlet the ring-width was enlarged.

All further tower components are conventional. The interior contains the water basin to collect the re-cooled water. Its basin plate and walls consist of water-proof RC 30/37 with 0.20 m of thickness, founded on a 0.15 m thick C 12/15 layer over an anti-freeze stratum of 0.30 m. The fill construction and the water distribution are designed as a prefabricated RC beam-column structure also made of high-performance concrete ARHPC 35/85.

The new Niederaussem power block BoA went into service in 2002, gaining excellent service experiences up to date. Presently, a series of new fossil fueled (lignite and hard coal) power stations is under design/construction in Germany since then, all with very similar NDCTs, and those common attributes mentioned at the beginning: Meridional shape optimization, cleaned flue gas release, ARHPC 35/85, design for durability. The lecture will present details of these attributes, and demonstrate design consequences of them, like preserving the original buckling safety, vibration properties and simulating the damage evolution over their life-times.

2. High "dry" cooling towers and low (mini) solar chimneys

Wet cooling systems consume cooling water through evaporation, as the vapor cloud above the tower indicates. If water consumption is unacceptable, "dry" cooling has to be chosen, in which the water is captured in a closed piping system. Then cooling works only by convection with lower efficiency, such that dry cooling towers have strongly enlarged dimensions. Already in the 1970ies large dry NDCTs were designed for power station in arid zones, reaching up to 300 m. With this height they approach low solar chimneys which start for professional operation at heights of approximately 500 m.

Figure 3 shows the design study of such a chimney. The tower has a total height of 500 m, diameters of 120 m at the throat and of 200 m at its base. The wall thickness increases from 0.25 m on the top to 0.60 m on the foundation slab. The shell with shape-optimized meridian requires a classical upper edge member and three intermediate stiffening rings. These stiffeners serve two important purposes,

- to reduce the buckling lengths of the shell for sufficient safety against instability failure,
- to constrain the meridional/shear forces in the shell due to wind towards a beam-like behavior.

The first purpose can be achieved with rather moderate sized cross-sections of all four stiffeners, attached on the shell outside, namely a hangover-width of 2.50 m and a thickness of 0.40 m. The second purpose requires stiffer rings in order to reduce the maximum wind tension towards the order of magnitude of the dead-load compression, an optimal design goal. With the above given dimensions, tension/shear stress maxima can be reduced up to 2/3. Higher reductions require internal spokes in the rings as recommended by (Schlaich *et al.* [4]).

Experienced designers of NDCT shells would attempt to construct the shell of Figure 3 without intermediate rings. The lecture will demonstrate for this case how the then globally extended instability modes require a thickness increase of the shell. Adding three sufficiently stiff intermediate rings, probably with spokes, as mentioned above lets the buckling safety of the shell grow by the factor 1.7.

3. Shells for future solar chimneys power plants

Due to Figure 4 Solar Chimney Power Plants (SCPP) consist of the glass-covered collector area, the turbogenerators for power conversion and the solar chimney. In the collector, solar radiation heats the collector ground and so warms up the enclosed air, which streams towards the center. There in the power conversion units, the energy of the air stream partly transforms into electric power, before being released through the chimney as pressure sink.

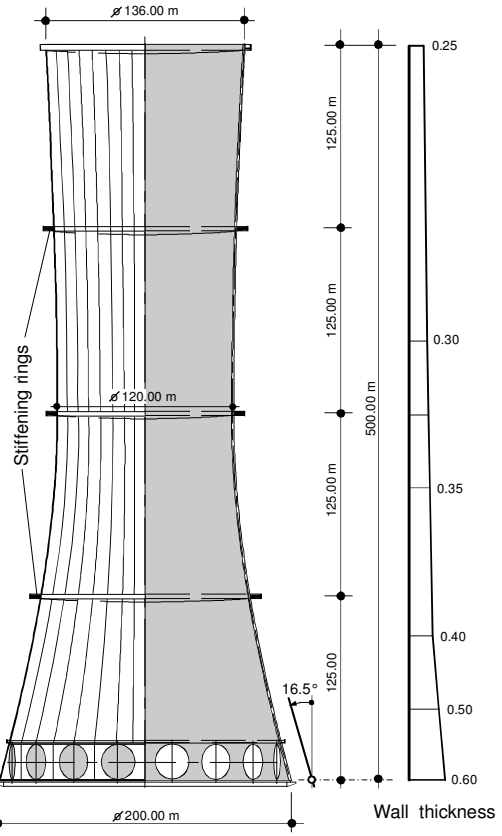

Figure 3: Solar tower of 500 m of height

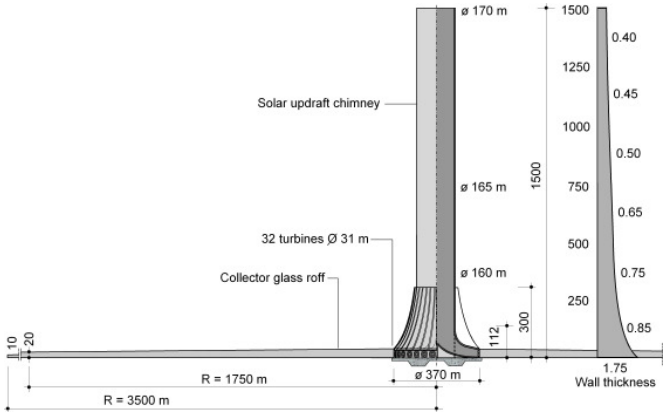

Figure 4: Overview over components of a SCPP

SCPPs are the most sustainable natural resources for electric power generation. They copy the daily solar-thermal air motion in the atmosphere producing electric energy completely free of CO_2-emissions. However, up to date none SCPP has been brought to reality, except for one 50 kW-prototype, erected 1982 in Spain under the guidance of J. Schlaich (Schlaich *et al.* [4]), a pioneer of this technology. This prototype power station worked successfully for more than 6 years. The efficiency of such power generation depends mainly on the size of the collector area and on the height of the chimney, both reasons for the enormous dimensions of SCPPs: Collector diameters up to 7 km and chimney heights up to 1500 m are on pre-design. Figure 5 shows a collection of several possible solar chimneys, all compared to the highest natural draft cooling tower at Niederaussem.

From a load-carrying viewpoint, solar chimneys are extremely enlarged, over-dimensioned NDCT shells, demonstrating all those problems known to cooling tower designers from half a century of experience, namely:

- High compression stresses under deadweight D, wind action W and service temperature T,
- tendency to vertical outside cracking under D, W and T,
- high sensitivity to shell buckling instabilities under D, W and wind suction S,
- forced wind vibrations in the upper chimney part eventually leading to dynamic instabilities,
- strong sensitivity to soil-structure interaction phenomena,
- interestingly a natural safety margin against seismic actions because of low 1st eigenfreqencies,
- stress and thermal fatigue phenomena of the required high-performance concrete,
- durability problems towards the end of a SCPP's service live duration (designed for 80÷120 years).

The structural design of such a solar chimney is an optimization process to compromise between several of these conflicting key points, as the presentation will point out (Backström *et al*. [1]). As example, Figure 6 shows the first three buckling modes for a 1000 m solar chimney with upper edge member and nine intermediate stiffening rings, designed for high performance RC 70/85.

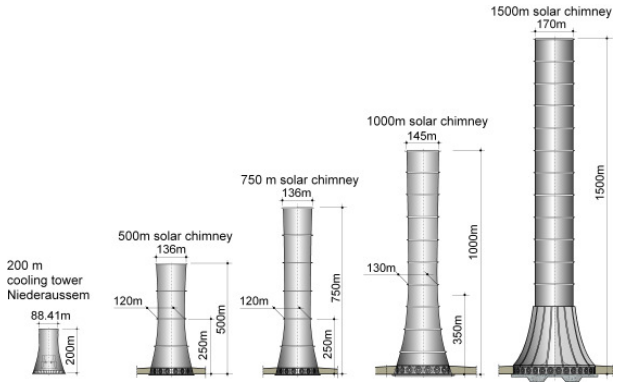

Figure 5: Solar chimneys of different height

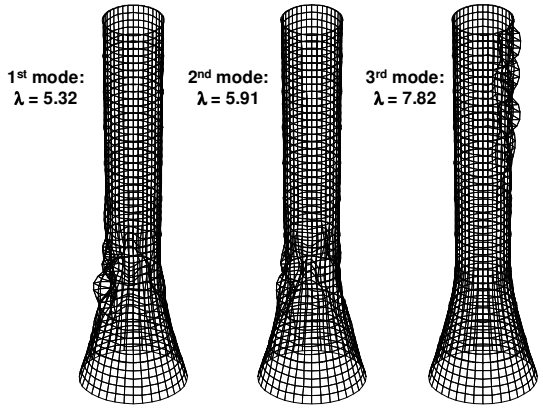

Figure 6: Buckling modes of 1000 m solar chimney

4. Summary

The presentation will illuminate the role of shell structures in power generation technology, in presence. Due to the worldwide rising consciousness for sustainable, CO_2-free energy production, this role is expected to grow enormously in future SCPPs.

Acknowledgement: The second author is deeply indebted to the Volkswagen Foundation, Hanover, for financial support. All authors thank Dipl.-Ing. M. Graffmann, Krätzig & Partner, for valuable contributions.

References

[1] Backström TW von, Harte R, Höffer R, Krätzig WB, Kröger DG, Niemann H-J, Zijl GPAG van. State and Recent Advances of Solar Chimney Power Plant Technology. Submitted to *PowerTech*.

[2] Busch D, Harte R, Krätzig WB, Montag U. New Natural Draft Cooling Tower of 200m of Height. *Engineering Structures* 2002; **24**: 1509-1521.

[3] Krätzig WB, Harte R, Lohaus L, Wittek U. Naturzugkühltürme (Natural draft cooling towers). Chapter X in *Betonkalender* 2007, Vol. 2, 231-322. Ernst & Sohn, Berlin.

[4] Schlaich J, Bergermann R, Schiel W, Weinrebe G. Design of Commercial Solar Updraft Tower Systems, Utilization of Solar Induced Convective Flows for Power Generation. *Journal of Solar Energy Engineering* 2005; **127**: 117-124.

Proceedings of the 6th International Conference on
Computation of Shell and Spatial Structures
IASS-IACM 2008: "Spanning Nano to Mega"
28-31 May 2008, Cornell University, Ithaca, NY, USA
John F. ABEL and J. Robert COOKE (eds.)

Answers to three not quite straightforward questions in structural stability

Andreas STEINBOECK, Gerhard HOEFINGER, Xin JIA, Herbert A. MANG*

*Institute for Mechanics of Materials and Structures, Vienna University of Technology
Karlsplatz 13/202, 1040 Vienna, Austria
herbert.mang@tuwien.ac.at

Abstract

In this contribution, the following three questions will be answered by means of both, theoretical proofs and practical examples:

- Are linear prebuckling paths and linear stability problems mutually conditional?
- Does the conversion from imperfection sensitivity into imperfection insensitivity by means of a modification of the original structural design require a symmetric postbuckling path?
- Is hilltop buckling, characterized by the coincidence of a bifurcation point and a snap-through point on a load-displacement path, necessarily imperfection sensitive?

1. Introduction

Despite the long history of structural stability as a field of great scientific relevance and practical importance, it holds a number of questions which so far were not rigorously answered. The reasons for some pieces of the structural stability landscape still being uncharted range from missing mathematical proofs to aspects that are commonly regarded as matters of course, which, at first glance, render thorough proofs dispensable. This is the motivation to ponder in this contribution over the three questions mentioned in the abstract.

They are related to the computation and study of load-displacement paths and, in particular, to *loss of stability phenomena*, exhibiting either *imperfection sensitivity* or *insensitivity* (Mang *et al*. [4]). After a brief theoretical introduction into the topic, theoretical answers to the posed questions will be given based on mathematical proofs. The lecture will supplement the theory by representative problems which were solved analytically and numerically, respectively.

2. Theoretical foundations

The behavior of a static, conservative system can be deduced from the *potential energy function* $V(\boldsymbol{u},\lambda):\mathbb{R}^N\times\mathbb{R}\rightarrow\mathbb{R}$. The vector $\boldsymbol{u}\in\mathbb{R}^N$ contains the displacement coordinates, implying that the system has N degrees of freedom. The parameter $\lambda\in\mathbb{R}$ is a load multiplier scaling a constant reference load $\boldsymbol{P}\in\mathbb{R}^N$. Therefore, $\boldsymbol{G}(\boldsymbol{u},\lambda):=V_{,\boldsymbol{u}}=\boldsymbol{F}^I(\boldsymbol{u})-\lambda\boldsymbol{P}$ may be interpreted as an out-of-balance force, which vanishes along any equilibrium path in the $\boldsymbol{u}$-λ-space. Here, $\boldsymbol{F}^I(\boldsymbol{u})\in\mathbb{R}^N$ is the vector of internal forces.

A crossing point $(\boldsymbol{u}_C,\lambda_C)$ of two equilibrium paths is called a *bifurcation point*. The equilibrium path containing the unloaded state is the *primary* or *prebuckling* path $(\tilde{\boldsymbol{u}}(\lambda),\lambda)$, the other one the *secondary* or *postbuckling* path.

The differential of $\boldsymbol{G}=\boldsymbol{0}$, i.e.,

$$\boldsymbol{K}_T\cdot d\boldsymbol{u}-d\lambda\boldsymbol{P}=\boldsymbol{0}, \tag{1}$$

with the symmetric *tangent-stiffness matrix* $\boldsymbol{K}_T := V_{,\boldsymbol{uu}}(\boldsymbol{u},\lambda)$, commonly serves as the basis for the solution of nonlinear structural problems by the FEM. Specializing (1) for the primary path, using the notation $\tilde{\boldsymbol{K}}_T(\lambda) := V_{,\boldsymbol{uu}}(\tilde{\boldsymbol{u}}(\lambda),\lambda)$, and disregarding, for the time being, snap-through points characterized by $d\lambda = 0$, (1) can be expressed as

$$\tilde{\boldsymbol{K}}_T \cdot \tilde{\boldsymbol{u}}_{,\lambda} - \boldsymbol{P} = \boldsymbol{0}, \tag{2}$$

or, after differentiation with respect to λ, as

$$\tilde{\boldsymbol{K}}_{T,\lambda} \cdot \tilde{\boldsymbol{u}}_{,\lambda} + \tilde{\boldsymbol{K}}_T \cdot \tilde{\boldsymbol{u}}_{,\lambda\lambda} = \boldsymbol{0}. \tag{3}$$

The secondary path is parameterized by a scalar η, with $\eta = 0$ corresponding to the bifurcation point $(\boldsymbol{u}_C, \lambda_C)$. The displacement offset between the primary and the secondary path is defined by the vector $\boldsymbol{v}(\eta) \in \mathbb{R}^N$. Thus, $\boldsymbol{u}(\eta) = \tilde{\boldsymbol{u}}(\lambda(\eta)) + \boldsymbol{v}(\eta)$ describes the displacement along the secondary path. Single-valuedness is guaranteed for $\boldsymbol{v}(\eta) : \mathbb{R} \to \mathbb{R}^N$ but not for $\tilde{\boldsymbol{u}}(\lambda) : \mathbb{R} \to \mathbb{R}^N$. Frequently, the coordinates are chosen such that η is a component of $\boldsymbol{u}$. Insertion of the series expansions

$$\lambda(\eta) = \lambda_C + \lambda_1\eta + \lambda_2\eta^2 + \lambda_3\eta^3 + \mathcal{O}(\eta^4) \tag{4}$$

$$\boldsymbol{v}(\eta) = \quad \boldsymbol{v}_1\eta + \boldsymbol{v}_2\eta^2 + \boldsymbol{v}_3\eta^3 + \mathcal{O}(\eta^4) \tag{5}$$

into the specialization of $\boldsymbol{G}$ for the secondary path, i.e., $\boldsymbol{G}(\eta) = \boldsymbol{G}(\tilde{\boldsymbol{u}}(\lambda(\eta)) + \boldsymbol{v}(\eta), \lambda(\eta)) = \boldsymbol{0}$, yields the new series expansion

$$\boldsymbol{G}(\eta) = \boldsymbol{G}_{0C} + \boldsymbol{G}_{1C}\eta + \boldsymbol{G}_{2C}\eta^2 + \mathcal{O}(\eta^3) = 0 \tag{6}$$

with $\boldsymbol{G}_{nC} = \boldsymbol{G}_{,\eta^n}|_{\eta=0}/n!$ $\forall n \in \mathbb{N}$. Since (6) must hold for arbitrary values of η, $\boldsymbol{G}_{nC} = \boldsymbol{0}$ $\forall n \in \mathbb{N}$. This condition paves the way for successive calculation of the unknowns $\boldsymbol{v}_1, \lambda_1, \boldsymbol{v}_2, \lambda_2$, etc. To render this calculation unique, the length of $\boldsymbol{v}_1$ has to be chosen (not equal to zero) and the orthogonality condition $\boldsymbol{v}_1 \cdot \boldsymbol{v}_i = 0$ $\forall i > 1$, suggested in Budiansky [2] can be materialized.

3. Are linear prebuckling paths and linear stability problems mutually conditional?

A primary path is *linear* if

$$\tilde{\boldsymbol{u}}_{,\lambda} = \boldsymbol{k} = \text{const.} \quad \forall \lambda \in \mathbb{R}. \tag{7}$$

Thus, $\tilde{\boldsymbol{u}}(\lambda) = \tilde{\boldsymbol{u}}(0) + \lambda\boldsymbol{k}$ with a constant (non-zero) vector $\boldsymbol{k}$. A stability problem is considered as *linear* if the tangent stiffness matrix specialized for the primary path can be written as

$$\tilde{\boldsymbol{K}}_T = \boldsymbol{K}_0 + \lambda\boldsymbol{K}_1, \tag{8}$$

with constant matrices $\boldsymbol{K}_0$ and $\boldsymbol{K}_1$ (cf. Zienkiewicz and Taylor [7]). Provided that the unloaded state $(\lambda = 0)$ is stable, $\boldsymbol{K}_0$ is positive definite. $\boldsymbol{K}_1 = \boldsymbol{K}_1^T$ may be any constant non-zero matrix. Consequently, $\det(\tilde{\boldsymbol{K}}_T(\lambda)) = 0$, i.e., the condition for loss of stability, is a scalar algebraic equation in λ, which facilitates the computation of the critical load level λ_C.

3.1 A linear prebuckling path is not sufficient for a linear stability problem

Utilization of (7) in (3) yields

$$\tilde{\boldsymbol{K}}_{T,\lambda} \cdot \boldsymbol{k} = \boldsymbol{0} \quad \forall \lambda \in \mathbb{R}. \tag{9}$$

Clearly, for any value of λ, $\boldsymbol{k}$ is a zero eigenvector of $\tilde{\boldsymbol{K}}_{T,\lambda}$. Yet, this is *not* sufficient for (8), i.e. (7) $\not\Rightarrow$ (8).

3.2 A linear stability problem is not sufficient for a linear prebuckling path

Substitution of (8) into (2) shows that for a linear stability problem, $\tilde{\boldsymbol{u}}$ is defined by the differential equation

$$(\boldsymbol{K}_0 + \lambda\boldsymbol{K}_1) \cdot \tilde{\boldsymbol{u}}_{,\lambda} - \boldsymbol{P} = \boldsymbol{0}. \tag{10}$$

The existence of an appropriate vector $\boldsymbol{k}$ such that (7) is a solution of (10) is *not* guaranteed. Thus, (8) $\not\Rightarrow$ (7), which is explained in more detail in Steinboeck and Mang [6]. Moreover, it follows from (10) that a linear stability problem entails a linear prebuckling path *only* if in addition $\boldsymbol{K}_1 \cdot \tilde{\boldsymbol{u}}_{,\lambda} = \boldsymbol{0}\ \forall \lambda$.

4. Does the conversion from imperfection sensitivity into imperfection insensitivity require a symmetric postbuckling path?

To achieve a conversion from imperfection sensitivity into insensitivity, the original structure must be modified. The degree of such a modification may be parameterized by means of a scalar κ. In many cases, it is of interest to find values of κ, for which the system is imperfection insensitive.

4.1 Conditions for symmetric load-displacement paths

For a definition of *symmetric* load-displacement paths, it is reasonable to start out from the potential energy function. As suggested in Steinboeck *et al*. [5], symmetry requires

$$V(\boldsymbol{u},\lambda) = V(\boldsymbol{T}(\boldsymbol{u}),\lambda) \quad \forall (\boldsymbol{u},\lambda) \in \mathbb{R}^N \times \mathbb{R}, \tag{11}$$

where the linear mapping $\boldsymbol{T}: \mathbb{R}^N \to \mathbb{R}^N$ is an element of a *symmetry group*. Moreover, symmetry of the secondary path with respect to η requires

$$V(\tilde{\boldsymbol{u}}(\lambda(\eta)) + \boldsymbol{v}(\eta), \lambda(\eta)) = V(\tilde{\boldsymbol{u}}(\lambda(-\eta)) + \boldsymbol{v}(-\eta), \lambda(-\eta)) \quad \forall \eta \in \mathbb{R}. \tag{12}$$

Condition (11) must hold along the primary path, and the uniqueness of this path implies $\tilde{\boldsymbol{u}}(\lambda) = \boldsymbol{T}(\tilde{\boldsymbol{u}}(\lambda))$. Moreover, a comparison of (11) and (12) reveals that $\lambda(\eta) = \lambda(-\eta)$ and $\boldsymbol{v}(\eta) = \boldsymbol{T}(\boldsymbol{v}(-\eta))$. These conditions may be summarized as follows:

A postbuckling path is said to be *symmetrical* with respect to η if it obeys the definition:

$$\lambda(\eta) = \lambda(-\eta) \quad \wedge \tag{13}$$

$$\boldsymbol{v}(\eta) = \boldsymbol{T}(\boldsymbol{v}(-\eta)) \quad \wedge \tag{14}$$

$$\tilde{\boldsymbol{u}}(\lambda(\eta)) = \boldsymbol{T}(\tilde{\boldsymbol{u}}(\lambda(\eta))). \tag{15}$$

It follows (trivially) from (4) that $\lambda_1 = \lambda_3 = \lambda_5 = \ldots = 0$ is a necessary condition for symmetry.

4.2 Conditions for imperfection insensitivity

According to Bochenek [1], a symmetric load-displacement behavior in the *vicinity* of $(\boldsymbol{u}_C, \lambda_C)$ and satisfaction of the inequality $\lambda_{,\eta}(\eta)\,\mathrm{sign}(\eta) \geq 0$ in an open *local* domain around $(\boldsymbol{u}_C, \lambda_C)$ are necessary and sufficient for imperfection insensitivity. In fact, $\lambda_{,\eta}(\eta)\,\mathrm{sign}(\eta)$ must not vanish in this local domain except at $(\boldsymbol{u}_C, \lambda_C)$. Therefore, with the help of $m_{\min} := \min\{m \mid m \in \mathbb{N}\setminus\{0\}, \lambda_m \neq 0\}$, a necessary and sufficient condition for *imperfection insensitivity* is found as

$$m_{\min} \text{ is even} \quad \wedge \quad \lambda_{m_{\min}} > 0. \tag{16}$$

If this condition is not satisfied, the system is *imperfection sensitive*.

4.3 A symmetric postbuckling path is not necessary for the conversion from imperfection sensitivity into imperfection insensitivity

A comparison of (13)-(15) with (16) shows that imperfection insensitivity is *independent* of (14) and (15). Thus, if the coefficients λ_i are computed up to an index $i = m$ such that $\lambda_m \neq 0$, (16) facilitates a decision about imperfection sensitivity or insensitivity. From these considerations it follows that a conversion from imperfection sensitivity into imperfection insensitivity is characterized by a sign reversal of $\lambda_{m_{\min}}$, which does *not* require symmetry.

Evidently, the choice of η is *not* unique, i.e. η may be replaced by means of a *bijective* coordinate transformation $\eta \mapsto \bar{\eta}(\eta)$ obeying $\bar{\eta}(0) = 0$. As it can be shown, satisfaction of (16) in the original system ensures that $\bar{m}_{\min}$ is even $\wedge\ \bar{\lambda}_{m_{\min}} > 0$ in the transformed system. As expected from a physical viewpoint, the (intrinsic) property of imperfection insensitivity (sensitivity) is invariant with respect to coordinate changes.

5. Is hilltop buckling necessarily imperfection sensitive?

Hilltop buckling is characterized by the coincidence of a *bifurcation* point and a *snap-through* point of a load-displacement path (Fujii and Noguchi [3]). The following gives a brief outline of determining whether the secondary path emerging from a hilltop buckling point is necessarily imperfection sensitive. For simplicity, the discussion is restricted to cases where $\lambda_1 = 0$, which is a necessary condition for imperfection insensitivity (cf. section 4).

In Mang *et al*. [4], the pivotal equation $\lambda_4 = a_1 \lambda_2^2 + b_2 \lambda_2 + d_3$ describing the relationship between λ_2 and λ_4 in terms of scalar coefficients a_1, b_2, and d_3 is deduced. In fact, if the structure under consideration is modified, a scalar design parameter κ defining the degree of the modification may be introduced (cf. section 4). Hence, the aforementioned equation turns out to be *parameter-dependent*, and the solution for $\lambda_2(\kappa)$ is obtained as

$$\lambda_2(\kappa)_{1,2} = -\frac{b_2(\kappa)}{2\,a_1(\kappa)} \pm \frac{\sqrt{b_2^2(\kappa) - 4\,a_1(\kappa)(d_3(\kappa) - \lambda_4(\kappa))}}{2\,a_1(\kappa)}. \tag{17}$$

Equ. (17) allows distinguishing between *two characteristic classes* of hilltop buckling problems. For the first class, $a_1 = -\infty$ and $b_2 = +\infty$. In the limit, $b_2 / a_1 = 0$, however the second addend of (17), with $d_3 - \lambda_4 = +\infty$, is negative in sign. Thus, for this class of problems, *all* load-displacement paths crossing the hilltop buckling point are imperfection *sensitive*.

The second class of hilltop buckling problems belongs to a category of buckling problems characterized by a vanishing discriminant for any value of κ, i.e. $b_2^2(\kappa) - 4\,a_1(\kappa)(d_3(\kappa) - \lambda_4(\kappa)) = 0$. Hence, $\lambda_2(\kappa)_{1,2} = -b_2(\kappa)/(2\,a_1(\kappa))$. For this class, $a_1 = -\infty$, $b_2 = -\infty$. In the limit, $-b_2 / a_1$ is negative in sign. Thus, as for the first class of problems, *all* load-displacement paths crossing the hilltop buckling point are imperfection sensitive.

For both classes of hilltop buckling, $-\infty < \lambda_4(\kappa) < 0 \;\forall \kappa$. Departing from hilltop buckling by increasing the value of κ, it is seen that $\kappa \to +\infty$ corresponds, for the first class, with $\lambda_2(\kappa) \to +\infty$ and $\lambda_4(\kappa) \to +\infty$, whereas, for the second class, with $\lambda_2(\kappa) \to +\infty$ and $\lambda_4(\kappa) \to -\infty$, indicating a worse quality of asymptotic initial postbuckling behavior, generally preceded by a worse quality of transition from imperfection sensitivity to insensitivity.

Acknowledgements

The authors thankfully acknowledge support by the Austrian Academy of Sciences. X. Jia also gratefully acknowledges support by Eurasia-Pacific Uninet.

References

[1] Bochenek B. Problems of structural optimization for post-buckling behaviour. In *Structural and Multidisciplinary Optimization* 2003; **25**/5-6:423-435.

[2] Budiansky B. Post-buckling behavior of cylinders under torsion. In *Theory of thin shells - Proceedings of the second IUTAM symposium*, Copenhagen, Denmark, 5-9 September. Springer: Berlin, 1967; 212-233.

[3] Fujii F, Noguchi H. Multiple hill-top branching. In *Proceedings of the 2nd International Conference on Structural Stability and Dynamics*, World Scientific, Singapore, 2002.

[4] Mang HA, Schranz C, Mackenzie-Helnwein P. Conversion from imperfection-sensitive into imperfection-insensitive elastic structures I: Theory. In *International Journal of Computer Methods in Applied Mechanics and Engineering* 2006; **195**:1422-1457.

[5] Steinboeck A, Jia X, Hoefinger G, Mang HA. Conditions for symmetric, antisymmetric, and zero-stiffness bifurcation in view of imperfection sensitivity and insensitivity. In *Computer Methods in Applied Mechanics and Engineering* 2008, in press, doi: 10.1016/j.cma.2008.02.016

[6] Steinboeck A, Mang HA. Are linear prebuckling paths and linear stability problems mutually conditional? In *Computational Mechanics* 2008, in press, doi: 10.1007/s00466-008-0257-3

[7] Zienkiewicz OC, Taylor RL. The finite element method, volume 2, solid mechanics. Butterworth-Heinemann: Oxford, England, 2000.

Proceedings of the 6th International Conference on
Computation of Shell and Spatial Structures
IASS-IACM 2008: "Spanning Nano to Mega"
28-31 May 2008, Cornell University, Ithaca, NY, USA
John F. ABEL and J. Robert COOKE (eds.)

Computational morphogenesis:
Its current state and possibility for the future

Hiroshi OHMORI*

*Nagoya University
Furo-cho Chikusa-ku Nagoya 464-8603, Japan
Email hero@dali.nuac.nagoya-u.ac.jp

Abstract

Computational morphogenesis is the word that is generally used for expressing those techniques or ways of thought by which the configuration or the system itself of the structures is generated mainly through the usage of the computers, which is realized on the firm foundation of both FEM as a tool of numerical analysis and various kinds of method based on relatively newly developed algorithms for structural optimization. Recently, it has been getting a considerable number of users such as structural engineers or engineering architects for the structural design of the actual buildings as well as the proposal for the architectural competitions. In this contribution, such state-of-the-art around the computational morphogenesis especially in Japan and the future prospect of the computational morphogenesis will be presented.

1. Introduction

From the viewpoint of structural design, it can be undoubtedly said that recent extraordinary rapid development of computers has been drastically changing their position at an unbelievably high speed. We already have had the simulation tools with which even highly complicated structural problems such as those containing geometrical as well as material nonlinearities should be simultaneously involved and, furthermore, even the cracking or the breaking of the materials should be correctly taken into account. Admirably precise computer simulations of the breaking process of reinforced concrete structures are good examples which clearly explain those situation. Moreover, it should be noted that truly innovative achievement in the field of structural topology optimization appeared in 1988, the fruit of which is called homogenization design method achieved by Bensoe and Kikuchi[1]. The author believes that it was really a breakthrough paving the way for utilization of structural optimization into the structural design, where methods based on the topology optimization are indispensable and essential. On the other hand, in almost the same period, Genetic Algorithms, one of the most efficient schemes for the arrangement optimization problem, has been developed and a lot of researches of the application of the algorithm have been started including those in the structural optimization. Genetic Algorithm has very distinctive characteristics such that it can deal with discrete variables with ease and, furthermore, plural solutions can be simultaneously obtained besides the best solution in the large. These characteristics of Genetic Algorithms are important when they are utilized as a tool of the structural design.

In this contribution, the present states of computational morphogenesis is surveyed where the fundamental methods such as truss topology optimization by Genetic Algorithms and both size and topology optimization by extended ESO (Evolutionary Structural Optimization) method are presented and, as the application of those methods, several projects, some of which are actually realized and the others proposed for the international competitions are shown. Moreover, methodology for the life cycle design (LCD) of structures is presented which are realized through the usage of Genetic Algorithms as the arrangement optimization tool in 4-D space, that is, the four dimension composed of three coordinates in physical space besides time. This is also a part of Computational Morphogenesis and the significance of LCD hereafter is expected to grow for the near future.

2. Computational Morphogenesis of Structures

2.1 Truss Structures

Genetic Algorithm (GA) is one of the most effective optimization methods, which enables us to handle discrete variables. Owing to this characteristic, we can handle the standardized structural elements from which the optimal combination for the objective structures is investigated. Another advantage on using GA is that it gives pleural optimums beside the single best optimum solution, characteristic of which is very suitable for the process of structural design because the users or the designers can choose their preferable solution from those solutions proposed through the optimization process. Figure 1 shows the typical results for the truss dome and the truss roof structures, where the topologies as well as the combination of those structural elements are generated through the optimization process by GA (Kawamura *et al*. [3]).

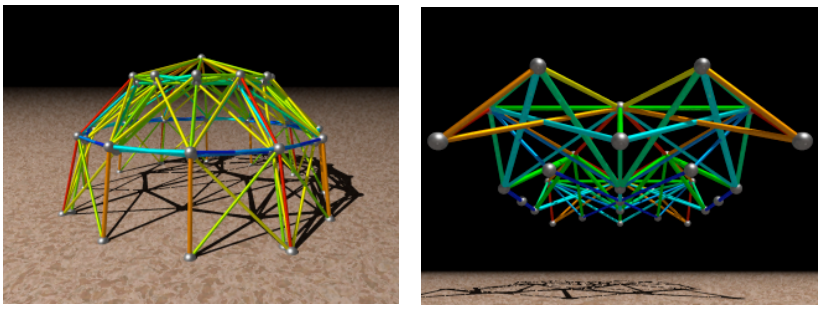

Figure 1: Truss Dome and Space Truss Structures Generated by GA

2.2 Continuum Structures

The author has proposed the Extended ESO (Evolutionary Structural Optimization) method by which we can obtain the solutions satisfying the constraint conditions required from the viewpoint of planning or other non-structural requirements. The Extended ESO method has been developed through several modifications on the original ESO method which has had been proposed by Xie and Steven [5]. Figure 2 shows the result of the shell structure having the minimum volume subjected to the concentrated load at the apex, where the limit of the displacement in the vertical direction at the loading point is provided (Cui *et al*. [2]). As shown in the figure, we can see that pursuing the minimum volume structure, through the use of the Extended ESO method, generates the organic configuration.

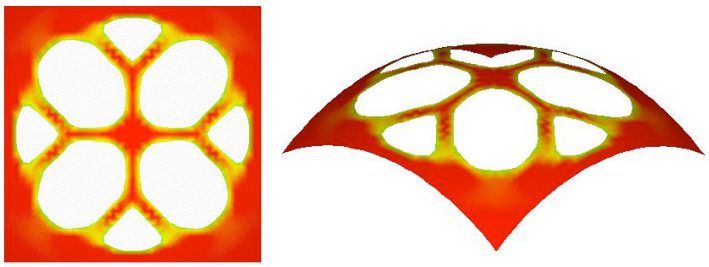

Figure 2: Shell Structure Generated by Extended ESO Method

The Extended ESO method which was originally developed and utilized for 2-D problems has been extended to the 3-D problems. In Figure 3, 3-D arch structure supporting the upper plate subjected to equally distributed load is shown, which has been generated through the 3-D extended ESO method.

On the other hand, the proposed Extended ESO method has been already applied to the structural design of the actual office building structure, the walls of which are designed based on the configuration generated by the extended ESO method as the initial design. Figure 4 shows the wall of the building as well as the intermediate process of the Extended ESO method (Ohmori *et al*. [4]), where we can see how the wall configuration has been changed through the modification process.

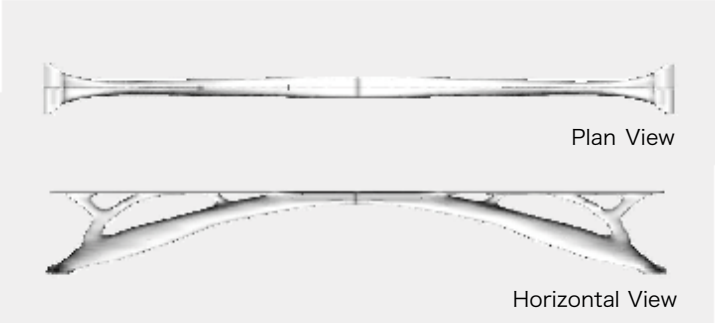

Figure 3: 3-D Arch Structure Generated by Extended ESO

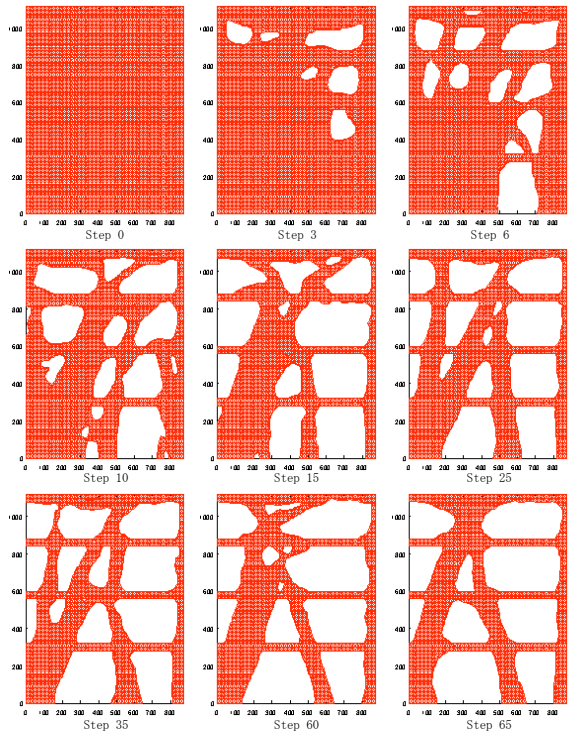

Figure 4: Structural Design of Wall through Extended ESO (Akutagawa Puroject)

3. Life Cycle Structural Design

It can be pointed out that most of conventional structures have been designed so that they can meet the requirements mainly coming from the initial performance from the viewpoint of their function, appearance as well as cost. However, the recent situation surrounding our environment has been drastically changing, that is, all industrial products should be produced as those whose impacts on the surrounding environment are reduced and controlled as possible as they can. Design of the structures is not an exception. Namely, we, structural engineers and designers, are requested to develop the design processes by which so-called sustainable structures are realized.

In this contribution, the authors propose the design method of the sustainable structures through the use of the optimization method by genetic algorithm, by which the optimal combinations of the structural elements as well as the optimal scenario of repair and preservation of the structures are obtained as the optimized solution (Figure 5). Generally, there are several objectives which have a trade-off relationship each other in life cycle design problems such as cost and structural performance. In those cases, the multi-objective optimization method can be effectively utilized and the multi-objective genetic algorithm is probably the most suitable technique for the

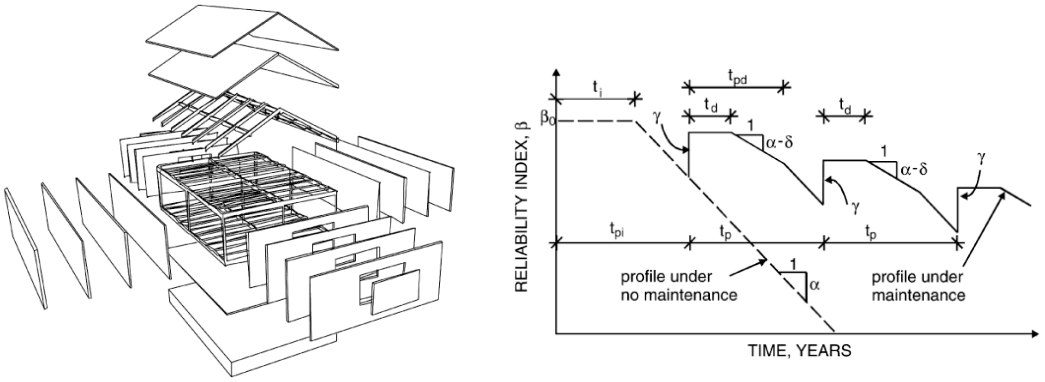

Figure 5: Life-Cycle Design of Structures

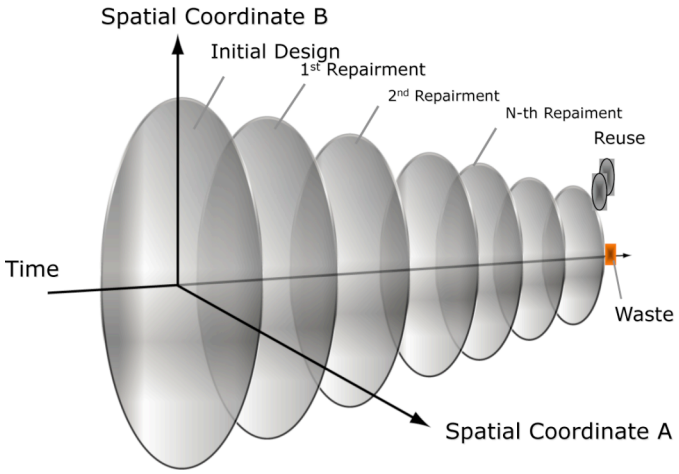

Figure 6: Arrangement Optimization in Time-Space Continuum

present problem. Figure 6 shows that the present multi-objective optimization problem toward the sustainable structures can be conceptually resulted in the optimization problem of the arrangement of the variables connected with the combination of structural elements as well as the time interval scheduling of the repair and preservation.

References

[1] Bensoe MP and Kikuchi N. Generating Optimal Topologies in Structural Design using a Homogenization Method, *Computer Methods in Applied Mechanics and Engineering* 1988; **71**: 197-224.

[2] Cui C, Ohmori H and Sasaki M, Computational Morphogenesis of 3D Structures by Extended ESO Method, *Journal of the International Association for Shell and Spatial Structures (IASS)* 2003; **44(1)**: 51-61

[3] Kawamura H, Osada S and Ohmori H. Genetic Creation of 3-Dimensional Truss Structures, *Journal of the International Association for Shell and Spatial Structures (IASS)* 2000; **41(3)**: 163-175.

[4] Ohmori H, Futai H, Iijima T, Mutoh A and Hasegwa Y. Computational Morphogenesis and its Application to Structural Design, *Proceedings of International Symposium on Shell and Spatial Structures, Theory, Technique, Valuation, Maintenance, Bucharest Poiana Brasov, Romania* 2005, 13-20.

[5] Xie YM and Steven GP. *Evolutionary Structural Optimization*, Springer Verlag, 1997.

Proceedings of the 6th International Conference on
Computation of Shell and Spatial Structures
IASS-IACM 2008: "Spanning Nano to Mega"
28-31 May 2008, Cornell University, Ithaca, NY, USA
John F. ABEL and J. Robert COOKE (eds.)

Folding and deployment of stored-energy composite structures

Sergio PELLEGRINO

California Institute of Technology
1200 E. California Blvd, MC 301-46, Pasadena CA 91125
sergiop@caltech.edu

Abstract

This lecture will present novel simulation techniques for lightweight deployable structures consisting of very thin sheets of fibre-reinforced composite materials. These structures are folded elastically and are able to self-deploy (dynamically) when they are released. Novel structural concepts of this kind were recently introduced on missions requiring parabolic reflector dishes for telecommunications and tubular deployable booms supporting sensors. A variety of related concepts are currently under consideration for future missions.

Designing these structures requires detailed predictions that capture both the overall, large displacement deformation of the structure, including the effects of contact and friction at the interfaces between parts of the structure that come into contact, and also the localised deformation of the most heavily deformed regions of the structure, in order to verify that no damage will occur in these regions.

Achieving this poses a number of novel challenges. First, the constitutive behaviour of thin composite materials differs fundamentally from that of standard composites and hence needs to be approached with suitable homogenization theories. Second, contact between heavily deformed (but still elastic) surfaces plays a key role in the tight packaging of these structures and the interaction between local and global instabilities that are encountered, even for the simplest configurations of current interest, is such that implicit solution schemes that attempt to capture the complexity of the physical situation become overwhelmed. Third, folding aids, such as jigs, straps, etc. are often used to facilitate the actual folding of a real structure without causing any damage and, although modelling this process in full detail is not necessary, any simulation needs to be steered through a maze of instabilities. The engineer must have confidence in the final predictions, because a fully detailed model of the folded configuration is required, to provide the initial conditions for any study of deployment.

Proceedings of the 6th International Conference on
Computation of Shell and Spatial Structures
IASS-IACM 2008: "Spanning Nano to Mega"
28-31 May 2008, Cornell University, Ithaca, NY, USA
John F. ABEL and J. Robert COOKE (eds.)

Rigid mechanics and its role in nonlinear structural analysis

Y. B. YANG*

*Department of Civil Engineering, National Taiwan University
Taipei, Taiwan 10617
E-mail: ybyang@ntu.edu.tw

Abstract

In the nonlinear analysis of elastic structures, the displacement increments generated at each incremental step can be decomposed into two components as the *rigid displacements* and *natural deformations*. Based on the updated Lagrangian (UL) formulation, the geometric stiffness matrix $[k_g]$ is derived for a 3D *rigid beam element* from the virtual work equation using a rigid displacement field. Further, by treating the three-node triangular plate element (TPE) as the composition of three rigid beams lying along the three sides, the $[k_g]$ matrix for the TPE can be assembled from those of the rigid beams. The idea for the UL-type incremental-iterative nonlinear analysis is that if the rigid rotation effects are fully taken into account at each stage of analysis, then the remaining effects of natural deformations can be treated using the small-deformation linearized theory. The present approach is featured by the fact that the formulation is *simple*, the expressions are *explicit*, and *all* member actions are considered in the stiffness matrices. The robustness of the procedure has been demonstrated in the solution of several problems involving the postbuckling response in previous papers by the author.

1. Introduction

In the past half a century, great advances have been made in nonlinear structural analysis. A partial review of related previous works can be found in Ref. [1], in which a total of 122 papers up to 2002 were cited. Based on the updated Lagrangian (UL) formulation, the purpose of this paper is to present a *conceptually simple*, but *procedurally robust*, incremental-iterative approach for the nonlinear analysis of elastic structures, by taking advantage of the different properties of each phase of the analysis [2,3].

For an incremental-iterative nonlinear analysis, two typical phases can be identified, i.e., the *predictor* and *corrector* phases. The *predictor* relates to solution of the structural displacement increments for given load increments based on the incremental structural equation, and the *corrector* is concerned with recovery of the force increments from the displacement increments for each element and the updating of the element forces [4]. The predictor affects only the speed of convergence of iteration, which therefore is allowed to be approximate to the extent that the direction of iteration is not midguided. In contrast, the corrector governs primarily the accuracy of solution, which should thus be made as accurate as possible. A common understanding is that if the corrector is not accurate anough, then the unbalanced forces calculated will be incorrect and the iterations performed to remove the unbalanced forces will be meaningless.

2. Logistics of incremental-iterative scheme

In nonlinear analysis of structures, we are faced with solution of equations of equilibrium of the incremental form, as given below:

$$[K]\{\Delta U\} = \{\Delta P\} \tag{1}$$

where $[K]$ is the tangent stiffness matrix, $\{\Delta U\}$ the displacement increments to be solved, and $\{\Delta P\}$ the load increments applied on the structure for the current incremental step. As for the incremental-iterative analysis, a schematic diagram of the mechanism involved is given in Figure 1. The slope *ab* represents the tangent stiffness of the structure used in the predictor for computing the displacement increments $\{\Delta U\}$, given the load increment $\{\Delta P\} = \{^2P\} - \{^1P\}$. Clearly, a convergent solution can always be obtained, regardless of whether the stiffness

matrix (i.e., the slope) is updated or not, as indicated in the figure. In fact, this phase affects only the direction of iteration or the number of iterations, but *not* the accuracy of solution.

In Figure 1, the segment *cd* represents the initial forces existing on each element, *de* the force increments generated during the increment, and *be* the unbalanced forces. Both the updating of initial forces, as represented by segment *de*, and the calculation of force increments, as represented by segment *be*, are part of the *corrector* phase. Clearly, the corrector must be accurate enough for the unbalanced forces to be correct. This is the logistics for performing an efficient incremental-iterative nonlinear analysis.

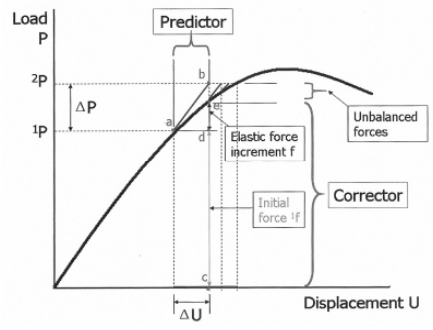

Figure 1: Idea of incremental-iterative analysis

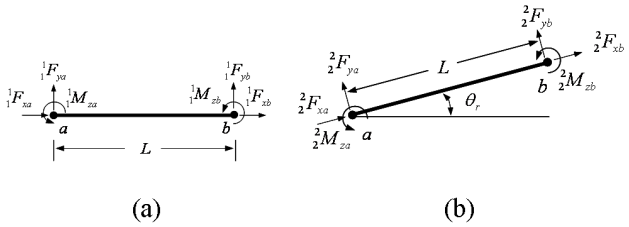

Figure 2: Initially stressed 2D beam: (a) before rigid rotation, (b) after rigid rotation

3. Rigid body rule

The rigid body rule is an important property that should be obeyed at all times in an incremental-iterative analysis, especially in the predictor and corrector phases. This rule requires that all the initial forces acting on an element should remain unchanged in magnitude and rotate following the rigid rotation. The result is the preservation of equilibrium of the element in the rotated position, as illustrated in Figure 2 [5,6].

4. Conventional finite element formulation

Based on the updated Lagrangian (UL) formulation, the virtual work equation for a finite element at C_2 but with reference to C_1 can be given in a linearized sense as [6]:

$$\int_V C_{ijkl}\,{}_1e_{kl}\,\delta\,{}_1e_{ij}\,dV + \int_V {}^1\tau_{ij}\,\delta\,{}_1\eta_{ij}\,dV = {}^2_1R - {}^1_1R \tag{2}$$

in which the first and second terms denote the strain energy and potential energy, respectively, V = volume, C_{ijkl} = constitutive coefficients, and ${}^1\tau_{ij}$ = Cauchy stresses of the element at C_1, δ = variation of the quantity following, and ${}_1e_{ij}$ and ${}_1\eta_{ij}$ = linear and nonlinear components of the strain increments with reference to C_1,

$${}_1e_{ij} = \frac{1}{2}\left(\frac{\partial u_i}{\partial x_j} + \frac{\partial u_j}{\partial x_i}\right), \quad {}_1\eta_{ij} = \frac{1}{2}\left(\frac{\partial u_k}{\partial x_i}\frac{\partial u_k}{\partial x_j}\right) \tag{3a,b}$$

where u_i = displacement increments and x_i = coordinates of the element at C_1. The external virtual works ${}^2_1R$ and ${}^1_1R$ at C_2 and C_1, respectively, can be related to the nodal loads $\left\{{}^2_1f\right\}$ and $\left\{{}^1_1f\right\}$ as

$${}^2_1R = \left\{\delta u\right\}^T\left\{{}^2_1f\right\}, \quad {}^1_1R = \left\{\delta u\right\}^T\left\{{}^1_1f\right\} \tag{4}$$

For a 3D beam element (Figure 3), the virtual work equation in Eq. (2) can be transformed into an *incremental stiffness equation* for the element from C_1 to C_2 as [6]

$$\left(\left[k_e\right]+\left[k_g\right]\right)\left\{u\right\} = \left\{{}^2_1f\right\} - \left\{{}^1_1f\right\} \tag{5}$$

where $\{u\}$ = displacement increments of the element. The *linear stiffness matrix* $[k_e]$ and *geometric stiffness matrix* $[k_g]$ can be derived as

$$\delta U = \int_V C_{ijkl}\,{}_1e_{kl}\,\delta\,{}_1e_{ij}\,dV = \left\{\delta u\right\}^T\left[k_e\right]\left\{u\right\}, \quad \delta V = \int_V {}^1\tau_{ij}\,\delta\,{}_1\eta_{ij}\,dV = \left\{\delta u\right\}^T\left[k_g\right]\left\{u\right\} \tag{6a,b}$$

By assembling Eq. (5) over all elements of a structure, we can obtain the structural equation as given in Eq. (1). In this study, we shall highlight that by choosing a robust incremental-iterative scheme, the use of the linear

stiffness matrix $[k_e]$, plus a *rigid-body qualified* geometric stiffness matrix $[k_g]$, is sufficient for solving a wide range of nonlinear problems.

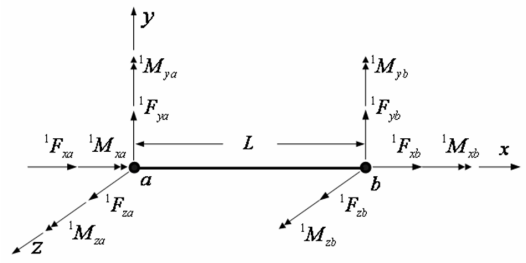

Figure 3: Three-dimensional beam element

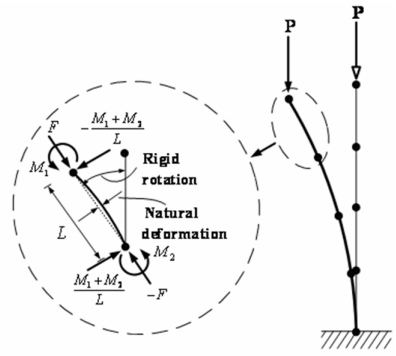

Figure 4: Rigid rotation and natural deformation

5. Concept of rigid rotation and rigid beam element

The displacements $\{u\}$ of each element of a structure in each incremental step can be decomposed into two parts as the *natural deformations* $\{u\}_n$ and *rigid displacements* $\{u\}_r$. In general, the *rigid displacements* constitute a great portion of the incremental displacements of each element (which are initially stressed) of the structure. In comparison, the magnitude of the *natural deformations* is relatively small for structures that are represented by a sufficient number of elements. Such a characteristic can be appreciated from the buckling of the cantilever shown in Figure 4.

For a rigid displacement field, the axial, twisting, and rotational displacements are constant, and the lateral displacements are linear, subjected to the constraints for the two ends that make the beam behave as a rigid or non-deformable body [2,3]. For this case, the strain energy in Eq. (6a) simply vanishes, i.e., $\delta U = 0$. One can derive from the potential energy term in Eq. (6b) a geometric stiffness matrix $[k_g]$ that is fully compatible with the rigid body rule. In Refs. [2,3], such a geometric stiffness matrix $[k_g]$ has been referred to as the stiffness matrix for the *rigid beam element*. One advantage with such an element is that it can be derived in a easy way and given in explicit form, while all member actions are duly taken into account.

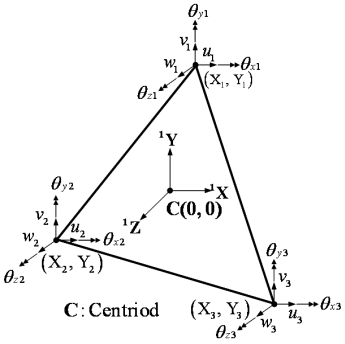

Figure 5: Three-node triangular plate element

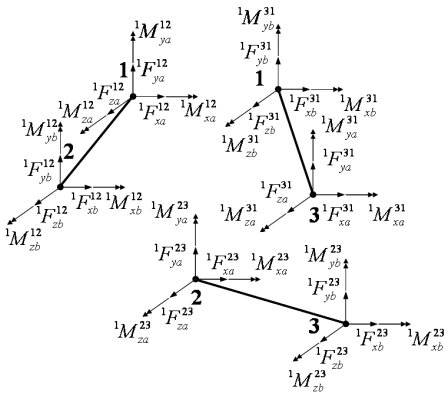

Figure 6: Forces and moments acting on each element

6. Triangular plate element (TPE) for plate and shell analysis

For the three-node *triangular plate element* (TPE) shown in Figure 5, there are three translational and three rotational DOFs at each node, thereby making each side of the element compatible with the 12-DOF beam element derived above. As far as the *rigid body behavior* of an element is concerned, only the *initial forces* acting on the element and the *external shape* of the element need to be considered. The elastic properties that are essential to the deformation of the element, such as Young's modulus, cross-sectional area and moments of

inertia, can be totally ignored. Based on such an idea, the rigid behavior of the TPE can be simulated as if it is composed of three rigid beams lying along the three sides of the element, as shown in Figure 6. It is by this concept that the geometric stiffness matrix $[k_g]$ for the rigid TPE was derived [3], which also appears to be explicit in form.

7. Stiffness matrices used in the predictor and corrector

As was pointed out previously, the structural stiffness matrix $[K]$ used in the predictor need *not* be exact and can be *approximate* in some sense, but must be accurate enough not to misguide the *direction of iteration* [7]. Such a point allows us to be released from the burden of deriving highly nonlinear elements, as conventionally attempted. It has been demonstrated in Refs. [2,3] that all we need for the predictor of an incremental-iterative analysis is the *linear stiffness matrix* $[k_e]$, made available from the linear theory, and the *geometric stiffness matrix* $[k_g]$ derived for the rigid element, for its qualification by the rigid body rule.

The *corrector* is concerned with recovery of the force increments $\{f\}$ from the displacement increments $\{u\}$ for each element and the updating of element forces at the end of the incremental step. For the case where each incremental step can be regarded as *small*, which is the case encountered by most nonlinear analysis, the element force increments $\{f\}$ can be computed with a sufficient level of accuracy using only the *linear stiffness matrix* $[k_e]$, and the initial nodal forces $\{{}^1f\}$ can be updated using the *rigid body rule* mentioned above. Clearly, the amount of computation involved in this phase is greatly reduced compared with the conventional approaches.

8. Concluding remarks

We have demonstrated that the geometric stiffness matrices can be derived for the 3D rigid beam element and rigid triangular plate element (TPE). It should be noted that in assembling the element stiffness matrices to form the structural matrix, joint equilibrium conditions should be established in the rotated position, as was described in Refs. [3,6], to account the effect of nodal moments undergoing rotations. In solving the postbuckling behaviors of structures using the prediction/corrector concept presented above, along with the rigid element and rigid body rule, it is essential that a reliable solution scheme be used. The scheme that has been demonstrated to be quite powerful is the generalized displacement control (GDC) method proposed in Ref. [8]. The applicability of the present procedure has been demonstrated in the solution of a number of nonlinear problems [2,3].

Acknowledgement

The research reported herein has been sponsored in part by the ROC National Science Council through a series of research projects to the author, including the one with grant No. 81-0410-E002-05.

References

[1] Yang YB, Yau JD, Leu LJ. Recent developments on geometrically nonlinear and postbuckling analysis of framed structures. *Applied Mechanics Reviews*, 2003; **56**(4): 431-449.

[2] Yang YB, Lin SP, Leu LJ. Solution strategy and rigid element for nonlinear analysis of elastic structures based on updated Lagrangian formulation. *Engineering Structures* 2007; **29**: 1189-1200.

[3] Yang YB, Lin SP, Chen, CS. Rigid body concept for geometric nonlinear analysis of 3D frames, plates and shells based on the updated Lagrangian formulation. *Computer Methods in Applied Mechanics and Engineering* 2007; **196**: 1178-1192.

[4] Yang YB, Leu LJ. Force recovery procedures in nonlinear analysis. *Computers and Structures* 1991; **41**(6): 1255-1261.

[5] Yang YB, Chiou HT. Rigid body motion test for nonlinear analysis with beam elements. *Journal of Engineering Mechanics* ASCE 1987; **113** (9):1404-1419.

[6] Yang YB, Kuo SR. *Theory and Analysis of Nonlinear Framed Structures* 1994; Prentice Hall, Englewood Cliffs, N.J.

[7] Kuo SR, Yang YB. Tracing postbuckling paths of structures containing multi loops. *International Journal for Numerical Methods in Engineering* 1995; **38**(23): 4053-4075.

[8] Yang YB, and Shieh MS, Solution method for nonlinear problems with multiple critical points. *AIAA Journal* 1990; **28**(12): 2110-2116.